Sputter yield reduction and fluence stability of numerically optimised nano-columnar tungsten surfaces

Christian Cupak,* Herbert Biber, Johannes Brötzner, Martina Fellinger, Florian Brandstätter, and Friedrich Aumayr
Institute of Applied Physics, TU Wien, Fusion@ÖAW,
Wiedner Hauptstraße 8-10/E134, 1040 Vienna, Austria

Alvaro Lopez-Cazalilla, Fredric Granberg, and Kai Nordlund
Department of Physics, P.O. Box 43, FI-00014 University of Helsinki, Finland

Paul S. Szabo
Space Sciences Laboratory, University of California,
7 Gauss Way, Berkeley, CA 94720, United States

Andreas Mutzke
Max–Planck Institute for Plasma Physics, Wendelsteinstrasse 1, 17491 Greifswald, Germany

Raquel González-Arrabal
Instituto de Fusión Nuclear "Guillermo Velarde" and Departamento de Ingeniería Energética,
ETSI de Industriales, Universidad Politécnica de Madrid,
C/ José Gutiérrez Abascal, 2, E-28006 Madrid, Spain

(Dated: June 5, 2023)

Nano-columnar tungsten surfaces were investigated with numerical techniques regarding their potential to reduce sputtering by ion bombardment. We simulated a large number of different configurations with the SPRAY sputtering code to identify an optimal geometry. For the test case of 2 keV Ar^+ irradiation, a specific configuration was found which led to a significant sputter yield reduction for all studied ion incidence angles. For example, reductions by ∼80 % in comparison to the sputter yield values for a flat tungsten surface were observed during irradiation along the surface normal. These properties appear beneficial for application on first wall materials in nuclear fusion devices. The optimised surface was further investigated with the molecular dynamics code PARCAS and the binary-collision-approximation code SDTrimSP-3D, which supported the choice of this configuration. Furthermore, dynamic erosion simulations using SDTrimSP-3D were conducted, which predict a relatively long-lasting persistence of the sputter yield reduction if the structure is exposed to higher fluences.

I. INTRODUCTION

Nuclear fusion is one of the most promising currently developed options for sustainable energy supply in the future, due to its high energy release during the fusion process, its sustainability and the absence of CO_2 emissions during operation. Nevertheless, one of the main constraints for its application in a future power plant is the demand for suitable reactor wall materials which are able to withstand the intense conditions foreseen in the reaction chamber[1–3]. There are currently two main approaches aiming to achieve nuclear fusion energy supply: magnetic confinement fusion (MCF) and inertial confinement fusion (ICF). In MCF, the fusion plasma interacts with wall materials via processes which cause quasi-stationary thermal loads of 10-20 MW/m^2, combined with short, extremely strong thermal transients up to the GW/m^2 range during edge-localized modes (ELMs) relevant for plasma-facing components (PFC) like the divertor[4,5]. Moreover, the divertor material will be exposed to large particle fluxes ($\sim 5\times10^{23}$ $m^{-2}s^{-1}$) and fluences ($\sim 10^{31}$ m^{-2}) , mostly of hydrogen isotopes and helium[6]. This interaction can produce serious damage in the PFC. In particular, the erosion of PFC due to ion bombardment is a current topic in the field of MCF[7–9]. Complex magnetic confinement systems are used in the Tokamak and Stellarator concepts, which aim to minimise the direct interaction of plasma ions with the walls of such devices. However, under these intense conditions, erosion is hard to prevent. Erosion on the atomic scale due to ion impact, known as sputtering, is recognised not only to limit the lifetime of PFC, but also to increase the impurity concentration of heavier elements in the fusion plasma, which decreases the reactor efficiency severely[10]. Therefore, materials which have favourable properties are wanted for PFC. Such properties include for instance a high thermal conductivity and melting temperature, low hydrogen isotope retention and a low sputter yield under ion bombardment.

In many modern MCF devices, conventional tungsten is already in use[11–13] as PFC material due to its advantages regarding the aforementioned properties. However, W presents drawbacks such as the capability to form fuzz under He impact[14]. Recently, it was demonstrated that nano-structured tungsten surfaces can (in comparison to conventional flat W) cause a beneficial effect on several key parameters, like mitigation of thermal stress under localised heat loads[15] or decreased fuzz-growth rates[16]. Especially for nano-columnar tungsten (NCW) and needle-like W dendrites, it was furthermore observed that sputtering due to ion irradiation can be significantly decreased[17,18]. Besides, preferential sputtering of PFC with mixed elemental composition could promote the growth of needle-like surface features during prolonged plasma exposition, which may lead to similar effects[19,20].

Our motivation is based on a previous study in which we have shown that for a given NCW surface, the geometry was the main driver for reducing the sputter yield under ion irradiation at various ion incidence angle conditions[18,21]. While those results already indicated favourable characteristics, an open question was whether the sputter yield could be further reduced by tuning the geometrical configuration of the nano-columns (NC). More specifically, the variation of the distance between NCs (or NC surface coverage) and their shape (aspect ratio) are of interest. From the experimental point of view, the latter can be adjusted by selecting specific conditions for the oblique-angle physical vapour deposition (PVD) process, especially the deposition angle and time[22,23], whereas the distance between NCs may be selected by seeding the substrate material prior to deposition[24,25]. One way of seeding is to use a laser beam, which would be also relatively easy to perform on commercial scales and has been demonstrated to be very efficient. However, the addition of such a substrate pre-treatment would increase the costs of material fabrication. Therefore, in this paper we study the influence of NC separation distance and their aspect ratio on the sputter yield using computer simulations, to further justify whether it is worthwhile to modify their appearance. To achieve this goal, we have calculated the sputter yield for a large number of different NCW surfaces under irradiation with seeding gas ions, i.e. 2 keV Ar^+, using the ray-tracing sputtering code SPRAY[26]. Further, to verify the results calculated with the SPRAY code, the sputter yield of a smaller collection of NCW surfaces was also selected for simulation with other programs, namely the binary-collision-approximation (BCA) code SDTrimSP-3D[27] and the molecular dynamics (MD) program PARCAS[28], to enable a direct comparison. Finally, we analyse the long-term stability of NCW surfaces at high fluences, by simulating the erosion during prolonged ion irradiation for the optimised NCW surface with the dynamic SDTrimSP-3D code. Such an estimation is highly relevant for selecting materials to be used in future MCF reactors[29].

II. MATERIALS AND METHODS

At first, some general definitions regarding the geometrical configuration of NCW surfaces are introduced. One key result of former studies was that relative geometric conditions were sufficient to explain the effects on sputtering, rather than precise consideration of absolute dimensions [18]. For better comparability in the course of this work, the geometry of different NCW surfaces was described by scale-independent parameters like the surface coverage density (ρ_{sc}) and the aspect ratio (r_a), which are defined in equations (1) and (2).

$$\rho_{sc} = \frac{A_{NC}}{A_{tot}} \tag{1}$$

$$r_a = \frac{h}{d} \tag{2}$$

For the surface coverage density ρ_{sc}, the parameters A_{NC} and A_{tot} represent the laterally covered area by NCs and the total lateral area of the inspected field, respectively. Therefore, selecting ρ_{sc} is equivalent to selecting a certain separation distance between the NCs if an absolute value for the NC diameter is known. For the aspect ratio r_a, the parameters h and d denote the NC height and diameter (e.g., as indicated in Figure 2). Based on earlier investigations of real NCW surfaces, typical absolute values for h were found in the range of several 100 nm, while d was approximately 50 nm. Still, it was intended to find a general solution (independent from absolute dimensions) by optimising NCW surfaces through varying ρ_{sc} and r_a. Considering that the range of our selected ions (2 keV Ar^+) in W is substantially smaller than the diameter of NCs ($\sim$2 nm versus 50 nm), the relative geometric parameters ρ_{sc} and r_a should be sufficient to model the geometric reduction effect on sputtering. This assumption was considered for all numerical methods employed in this work, which are discussed in more detail later. In principle, the choice of a geometric and scale-independent treatment is motivated by the assumption that no projectile transmission or even rear-side sputtering can occur in the NCW surface. To decide whether these assumptions are applicable for a given case, one option is to calculate the scale-independent ratio τ by division of the projected projectile range R_p over the absolute NC diameter d, as shown in equation (3).

$$\tau = \frac{R_p}{d} \tag{3}$$

For each combination of projectile and target species and kinetic energy, there exists a specific threshold ratio τ_t, which corresponds to the minimum thickness of a material to prevent any transmission or rear-side sputtering. To check whether there is even a universal threshold ratio τ_t, the SDTrimSP code[30] was used together with a user-friendly GUI[31] to simulate projected ranges for a variation of projectile species and kinetic energies E_{kin}. W

TABLE I. Simulated projectile ranges for various projectile species and kinetic energies, the minimum thicknesses of W to prevent transmission events and the corresponding threshold ratio τ_t. The target material was kept as W and the incidence angle to 0° with respect to the surface normal. The data was obtained from SDTrimSP[30], with the aid of a user-friendly GUI[31].

E_{kin} and species	R_p [nm]	d_{min} [nm]	τ_t
2 keV Ar	2.34	10.5	0.22
10 keV Ar	6.29	26.0	0.24
2 keV D	22.03	82.0	0.27
10 keV D	77.42	240.0	0.32
5 keV C	9.84	35.0	0.28

was kept as target material. For each case, the thickness of the target was gradually adapted, until the minimum thickness d_{min} was reached which just prevented projectile transmission or rear-side sputtering. The simulated data is summarised in Table I.

As can be seen from the data on τ_t in Table I, the values for the studied cases vary between 0.22 and 0.32. It should be mentioned that a relatively large variation of kinetic energy and projectile mass was chosen, while τ_t remains similar. We select the smallest occurring value of 0.22 as a conservative choice to stipulate a general threshold ratio τ_t, indicating that for any combination of target and projectile species or kinetic energy, the actual ratio τ should be significantly smaller than 0.22 to ensure that a geometric and scale-independent treatment of sputtering is adequate. The projected range of 2 keV Ar in W ($R_p = 2.34$ nm) and the diameter of NCs ($d = 50$ nm) as relevant in the presented study allow to calculate a ratio of $\tau = 0.047$, which is substantially smaller than the aforementioned threshold value.

A. SPRAY

SPRAY is a sputtering simulation code which employs a ray-tracing algorithm to calculate sputter yields of rough surfaces[26]. In this model, quantities like sputter yields, ion reflection coefficients and vectors for emitted particles are initially required, e.g., by BCA-codes like SDTrimSP[30] for a flat surface as a repository data set. This repository data is then used during the execution of SPRAY, together with an input for the surface topography. Based on the repository data, the ray-tracing algorithm calculates sputtering at local surface segments, as well as redeposition of sputtered atoms and secondary sputtering by locally reflected ions. This approach allows to consider geometric effects like shadowing and redeposition of sputtered particles. In contrast to other numerical models, a main advantage of SPRAY is that the topography of interest is not limited in size, i.e., the calculation is independent on length scale of the surface data. Furthermore, the calculation of sputter yields is much faster than for other codes capable of considering 3D topographies. This efficiency enables to investigate a very large number of different surfaces or ion incidence angles using only a conventional desktop PC without need of cluster infrastructure. More information on the functionality of SPRAY can be found in literature[26].

In the course of this study, SPRAY was dominantly used to calculate the dependence of the sputter yield (under 2 keV Ar^+ irradiation) as a function of the surface coverage density ρ_{sc} and the aspect ratio r_a. The main aim was to find the configuration which leads to the lowest sputter yield at variable ion incidence angles. To this end, more than 100 different NCW surfaces were generated with a Python program on the basis of a template NCW model structure, with different ρ_{sc} (from 0.01 up to 0.9) and r_a (from 0.1 up to 25). A random selection of the parameters was sampled from this regime. For the template NCW surface, a good agreement between experimental and numerical data for sputtering was found[18]. To further maintain this comparability with experiments, also the same repository data set for 2 keV Ar^+ irradiation of W was used in SPRAY. The parameter ρ_{sc} was varied by tuning the separation width between the NCs. The variation of r_a was achieved by modification of the mean NC height. It should be mentioned that not all NCs had the same height, but a small random height variation ($\sim$10 nm) was introduced to enhance the qualitative appearance in respect to real NCW surfaces. The diameter of NCs was kept at 50 nm for all surfaces, which is much larger than the expected ion range in tungsten. Figure 1 shows a representative image of such NCW surfaces, which corresponds to an approximate ρ_{sc} of 0.10 and r_a of 10. The NCs were located at regular grid points on the surface, which could allow a fraction of incoming ions to propagate directly to the bottom surface if they travel along the grid axes direction. The artificial symmetry in our NCW surfaces was therefore statistically mitigated by randomly selecting the azimuthal ion impact direction for each individual ion.

B. SDTrimSP-3D

SDTrimSP-3D is a BCA-based sputtering simulation code, which enables to perform both static and dynamic calculations[27]. In this code, which can be seen as an extension of SDTrimSP[30], individual projectiles are launched towards a 3D topography, each causing a collision cascade with target atoms in the material. The trajectories of all collision partners are traced and for each collision, elastic energy and momentum transfer are calculated. The mean free path between collisions is selected on the basis of the target material density, while the impact parameter is selected randomly. The KrC interaction potential was used for simulating elastic nuclear collisions[33], which can be seen as the recommended option in SDTrimSP-3D for many ion-target combinations. Using the interaction potential and the impact

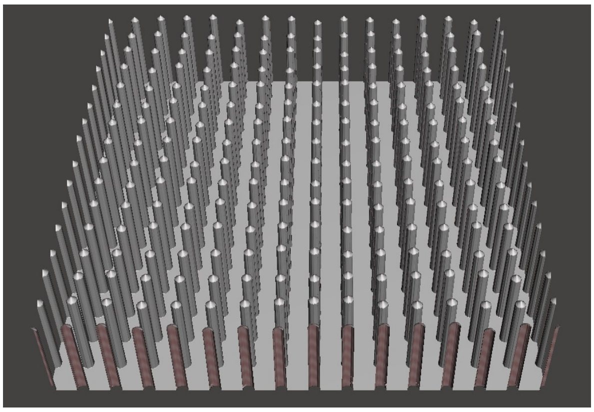

FIG. 1. Representative NCW surface which was used as input to SPRAY. In total, more than 100 different configurations with variable r_a (NC height / NC diameter) and ρ_{sc} (area laterally covered by NCs / total area) were generated, in order to identify the configuration leading to the lowest sputter yield. This visualisation was obtained with the free Meshmixer software[32].

parameter, the classical scattering integral can be solved numerically, which enables calculating scattering angles as well as energy and momentum transfer. Between collisions, electronic stopping is considered (e.g., by using the mean electronic stopping predicted from the models of Lindhard-Scharff[34] and Oen-Robinson[35]), which continuously decreases the kinetic energy of the moving atoms. Target atoms that propagate back towards the surface with enough kinetic energy to overcome the surface binding energy are emitted as sputtered atoms. It is important to highlight that SDTrimSP-3D is a more direct simulation method than the ray-tracing code SPRAY, as it allows to calculate individual collision cascades and directly includes redeposition, reflection or transmission events. Furthermore, the dynamic mode allows to investigate changes of the topography from continuous sputtering, which is another advantage. Due to computational constraints in terms of memory, the size of the topographical input is usually limited to several hundreds of nm in each dimension. However, since our PC offered relatively large memory, we were able to load a relatively large subsection of the NCW topography which was also used for SPRAY directly into SDTrimSP-3D . Given the fact that SDTrimSP-3D also enables periodic boundary conditions for the topography, the size of the input was considered to be sufficient. Since especially the dynamic calculations demand significant computational time, we only selected the optimised NCW surface and a single ion incidence angle $\theta = 60°$ for investigation of the fluence-dependent sputtering behaviour. The calculation time benefited also from the choice of 2 keV Ar^+ ions, which caused a substantial erosion already at relatively low fluence. A conventional desktop PC with an AMD Ryzen 9 5950X processor (7 of 32 threads used) and 128 GB RAM (fully used) was employed to perform the simulation. Besides, direct sputtering of the bottom surface was mitigated by selecting a specific azimuthal ion incidence angle $\varphi = 35°$ with respect to the global y-axis (later indicated in Figure 6c). More information on the principles of SDTrimSP-3D can be found in literature [27].

C. PARCAS-MD

The molecular dynamics (MD) simulations were carried out using the PARCAS code[28]. MD calculates the trajectories and forces of the atoms integrating Newton's equations of motion, considering an interatomic potential which rules the interactions between the atoms in the system. The description of these interactions is considerably accurate since it is parameter-free. However, it has a high computational cost compared to other methods used in this work. Hence, there is a limitation in time and size of the cell considered.

In the present work, we follow a similar methodology like in previous works[18,21]. W atoms interact with other W according to the Marinica potential[36]. In addition, the DMol potential[28] was used to describe the Ar-W and Ar-Ar interactions. Electronic stopping power was considered for those atoms which had a kinetic energy above 10 eV. Periodic boundary conditions were applied in the x- and y-directions, while the surface in the z-direction was open and crystallographically oriented as a (1 0 0) surface. The temperature used in the simulations was 300 K. Three different regions were defined in the cell to perform the irradiation: First, a fixed region with a small number of atomic layers at the bottom was considered, to prevent movement of the simulation cell. Then, some atomic layers were added, where a Berendsen thermostat[37] was utilised to control the temperature (NVT ensemble) on top of the fixed region. Finally, an NVE ensemble was used for the remaining simulation cell.

Four different NCW structures were designed from a (1 0 0) surface (see Figure 2 for the indication of dimensions) and relaxed at 300 K prior to irradiation. The actual dimensions were adapted for the individual simulation cells to meet different aspect ratios r_a and surface coverages ρ_{sc} (see Table II). The 2 keV Ar^+ irradiation of the cells was performed sequentially as in former studies[18,21,38,39] at incidence angles of $\theta = 0°$, 37°, 60° and 80° with respect to the surface normal, using a fixed azimuthal angle of $\varphi = 45°$ with respect to the y-axis (compare coordinate system in Figure 2). For each incidence angle, the same number of 2000 impacts was performed on all cells, which was selected for both achieving satisfying statistics and reasonable computational costs. Due to the same reason, the size of the NCW cells in MD needed to be scaled down by a factor of 50 in relation to the original size. Nevertheless, in a previous work also focusing on Ar^+ and W as projectile and target material, respectively[18], it was shown that for smaller diameter and size, keeping relative geometrical parameters like the surface coverage ρ_{sc} was sufficient to compare MD results well with data from both experiments and

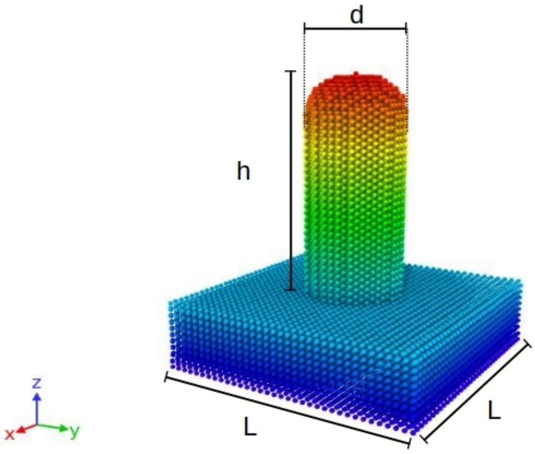

FIG. 2. Configuration of a representative MD simulation cell. The dimensions of the cell are marked as L, h and d, for bottom layer size, NC height and NC diameter, respectively. The colour gradient indicates the height from the bottom (blue) to the top (red).

TABLE II. Summary of geometric dimensions for all MD simulation cells (MD-1 to MD-4).

	MD-1	MD-2	MD-3	MD-4
L [Å]	84.5	110	126	94
h [Å]	300	100	113	113
d [Å]	30	40	70.6	77.2
A_{tot} $(L \times L)$ [Å^2]	7140.3	12100	12769	8836
A_{NC} $(\pi \times (\frac{d}{2})^2)$ [Å^2]	706.9	1256.6	3915	4681
ρ_{sc}	0.10	0.10	0.31	0.53
r_a	10	2.5	1.60	1.46

SPRAY. Furthermore, no severe effects due to the different target implementation (MD considers a crystalline W target in contrast to an amorphous structure in BCA) were observed, but it should be kept in mind that some differences in the sputtering properties for crystalline and amorphous targets can be in principle expected, as literature shows[40].

III. RESULTS

A. Optimisation results for NCW surfaces by SPRAY

The results for the NCW optimisation with SPRAY are presented for three ion incidence angle cases: $\theta = 0°$, $60°$ and $80°$ in respect to the global surface normal direction. These angles were chosen to investigate characteristic regimes before and beyond the maximum of the sputter yield dependence as a function of incidence angle, as known for a flat W surface under Ar$^+$ impact (see e.g. later in Figure 5(b)). Scatter plots were used to visualise the dependence of the sputter yield on ρ_{sc} and r_a for different NCW surfaces in Figure 3. For better comparability between the individual cases, the relative sputter yield normalised by the value for a flat W surface during 2 keV Ar$^+$ impact under the relevant incidence angle θ is plotted. For all incidence angles, a similar global trend is visible. While the gradient varied between the individual cases, larger ρ_{sc} and lower r_a generally lead to higher sputter yields (i.e., for the data points in the lower right quadrant). For smaller ρ_{sc} and higher r_a, a reduction of the relative sputter yield is found. For $\theta = 0°$, even a reduction down to 20 % of a flat W surface was observed (see Figure 3 (top)). This regime is indicated by a dashed magenta-coloured ellipse in all sub-plots. To guide the eye, also a horizontal line of dashed magenta was added for $r_a = 10$. This corresponds to an aspect ratio which was already demonstrated for a real NCW surface in a previous study[18]. For the specific case of $\rho_{sc} = 0.58$, data from experiments is available (star-shaped data points,[18]), which shows good agreement with the numerically simulated tendency. For even lower values of ρ_{sc} ~0.01, the SPRAY simulated sputter yield is rising again in Figure 3 (top), which appears intuitive, since in this asymptotic regime the NCs are very distant from each other. This behaviour is supporting that the characteristics of a flat surface become dominant (indicated by the blue boundary). However, considering the case of $\theta = 80°$, the sputter yield would drop even further for lower values of ρ_{sc}. This indicates that the optimum of ρ_{sc} is dependent on the incidence angle case. It should be mentioned that only few data points are available in the regime close to the blue boundary, limiting a more comprehensive discussion. Nevertheless, if the properties regarding sputter yield reduction for all presented incidence angle cases are considered, those parameters within the magenta-coloured ellipse show the overall best performance. It is important to mention that under $\theta = 80°$ (Figure 3 (bottom)) also sputter yield enhancement can happen for many geometric configurations. Still, if ρ_{sc} and r_a remain within the magenta-coloured ellipse, a decent sputter yield reduction is always preserved.

B. Results by MD, SPRAY and SDTrimSP-3D

Results on sputter yields from MD simulations, which are visualised in Figure 4, are compared for a selected ensemble of different NCW surfaces. Due to computational constraints, only a limited number of configurations could be inspected with MD, but for these we calculated sputter yields for a variable ion incidence angle θ between 0° and 80° with respect to the surface normal. The labels in the figure legend indicate the corresponding ρ_{sc} and r_a values of the NCW surfaces, in analogy to the parameters listed in Table II. It can be observed

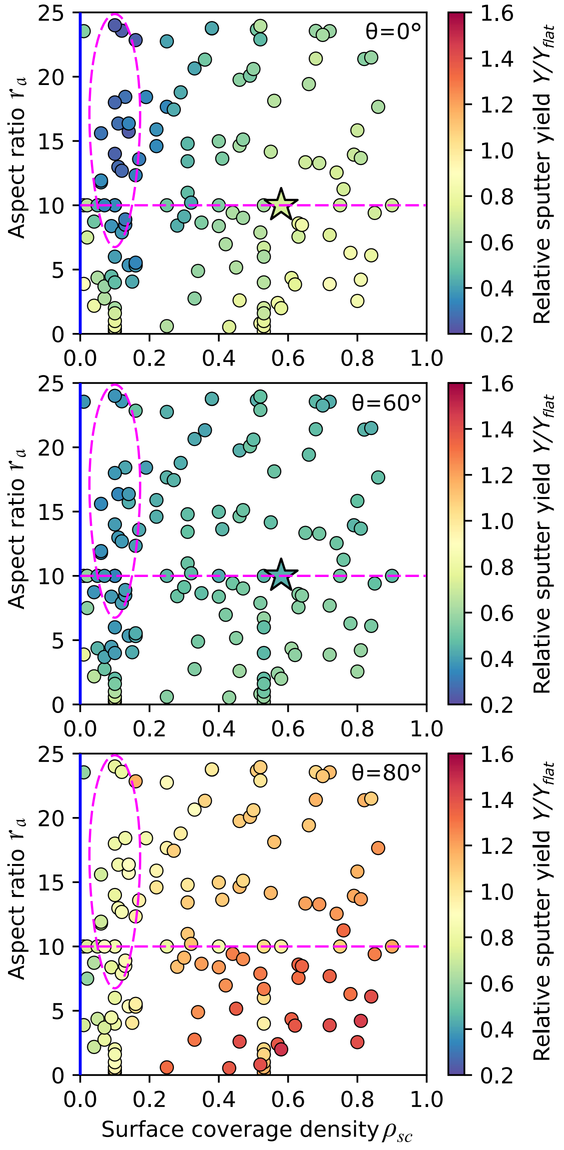

FIG. 3. Relative sputter yield under irradiation with 2 keV Ar$^+$ for NCW surfaces with variable aspect ratio r_a and surface coverage ρ_{sc}. Top: θ = 0°, centre: θ = 60°, bottom: θ = 80° ion incidence angle. The values in the colour bars were normalised by the sputter yields of a flat W surface (simulated by SDTrimSP[30]). The magenta coloured ellipse indicates a regime with favourable reduction. The horizontal line represents an r_a value which was technically achieved in a former study, where also experimental sputter yield data was obtained (star)[18]. The blue boundary indicates the asymptotic regime where the topography approaches a flat W surface.

that for decreasing ρ_{sc} and increasing r_a, MD predicts continuously lower sputter yields for the full range of ion incidence angles. This is in very good qualitative agreement to the tendencies observed in the previously shown results on NCW optimisation by SPRAY (Figure 3). For the special case of ρ_{sc} = 0.10 and r_a = 10, SDTrimSP-3D (red dotted), SPRAY (red dashed) and MD data (red solid) are included in Figure 5, besides SPRAY data for a flat W surface (black dashed). The latter data set is a reproduction of SDTrimSP, as a flat surface input does not affect the sputtering properties in SPRAY. For SPRAY and SDTrimSP-3D data based on the NCW surface, a very similar trend was found in the sputter yields, with only minor deviations close to 0° ion incidence angle. Considering the MD data set, besides a small offset in relation to SPRAY and SDTrimSP-3D towards even smaller sputter yields, the general tendency is also matching well. Therefore, we note that these sputter yield data follow the same trend, independent of the utilised simulation code. In addition, the data from all codes show a substantial reduction of the sputter yield in comparison to the flat surface over all ion incidence angles.

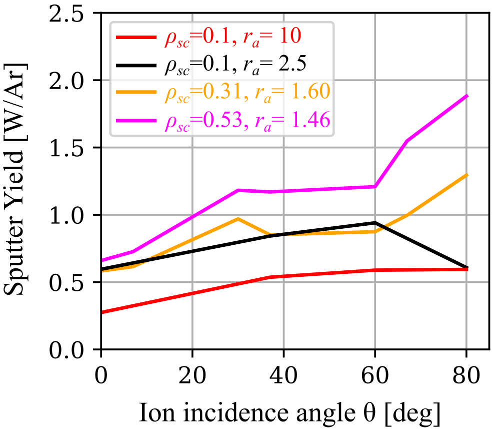

FIG. 4. MD simulated W sputter yields under 2 keV Ar$^+$ irradiation as a function of the ion incidence angle θ. A comparison of data for selected surfaces (MD-1 to MD-4) with given ρ_{sc} and r_a is shown.

C. Dynamic erosion with SDTrimSP-3D

The results from dynamic SDTrimSP-3D simulations are presented in Figures 6 and 7. An ion incidence angle of $\theta = 60°$ with respect to the surface normal and $\varphi = 35°$ with respect to the y-axis were used (compare the coordinate system in Figure 6c), while the latter was selected to prevent direct ion impact on the bottom surface along the free channels between NCs. The total fluence was set to 4.8×10^{21} Ar/m^2. The same optimised NCW surface input as predicted by SPRAY (ρ_{sc} = 0.10 and r_a = 10) was used for SDTrimSP-3D, while it was necessary to select a smaller lateral selection due to limited memory size (i.e., 8×8 NCs compared to 16×16 NCs in SPRAY). The topography (covering a lateral area of 1120×1120 nm) was discretised with voxels of 2.5 nm. The initial surface structure can be inspected in Figure 6a). In sub-figures b) and c), the dynamically eroded NCW surface is visu-

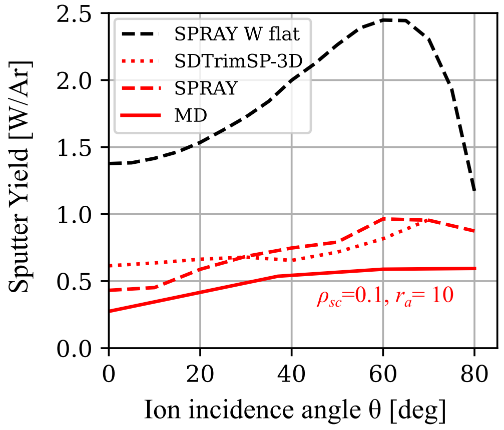

FIG. 5. Simulated W sputter yields as a function of the ion incidence angle θ for a flat W surface and the optimised NCW surface (with ρ_{sc}=0.1 and r_a=10). A comparison of simulated data from SDTrimSP-3D, SPRAY and MD is shown.

alised after an applied fluence of 1.8×10^{21} and 4.0×10^{21} Ar/m^2, respectively. The latter figure also shows a reference coordinate system with the angular ion incidence conditions. It can be clearly seen that the height of NCs is continuously reduced with increasing fluence. Modifications of the NC top shape resulted from sputtering and redeposition of W atoms. After a fluence of 1.8×10^{21} Ar/m^2 (see 6b)), also the bottom W surface became exposed to the incoming ion beam and was therefore sputtered directly. In Figure 6c), after 4.0×10^{21} Ar/m^2, it can be observed that the NCs were fully eroded, while the remaining topography resembles "ripples", oriented towards the azimuthal direction of incoming ions (35° with respect to the y-axis in Figure 6c)). A video of the continuous erosion can be found in the supplementary material.

The dynamic change of the surface topography had an effect on the sputter yield, which could be extracted for each simulated fluence increment. The fluence-dependent sputter yield obtained from this SDTrimSP-3D simulation is visualised in Figure 7. For comparison, the SDTrimSP-3D simulated sputter yield for a perfectly flat W surface under 2 keV Ar$^+$ irradiation at θ = 60° is shown (dashed red line). In addition, a sputter yield under identical irradiation conditions assuming a conventional rough W surface with a mean inclination angle δ_m = 45.5° (predicted by the empirical fit formula in reference[26]) is included (dashed orange line) to support the discussion later. The black dashed lines with labels b) and c) indicate the fluence values which correspond to the surface visualisations in Figure 6. While the sputter yield of NCW remains well below the value of a flat W surface during the whole simulation, a continuous increase is visible over rising fluence. The increase is initially slower, up to ~1.8×10^{21} Ar/m^2 (see dashed black line at b). Then, the increase of the sputter yield over rising fluence becomes steeper. In both cases, a linear fit can be made to approximate the data tendency. As depicted in Figure 7, the sudden change in the sputter yield slope over fluence allows to identify two different regimes (I and II). In regime I, a sputter yield slope of 6.8×10^{-23} W·m^2/Ar^2 could be calculated, while in regime II, a higher slope of 2.1×10^{-22} W·m^2/Ar^2 was deduced. These regimes correlate with the qualitative change of the NCW topography and the efficiency of NCs for protecting the bottom surface from direct ion impact. It is worthwhile to mention that, surprisingly, even though NCs were fully eroded after a fluence of 4.0×10^{21} Ar/m^2 (black dashed line c), no significant change in the sputter yield's slope over increasing fluence is observed.

IV. DISCUSSION

A. Optimisation of NCW by SPRAY

For all incidence angle cases, SPRAY simulations predicted the largest reduction of sputter yields for those NCW surface parameters within the magenta-coloured ellipse in Figure 3. In the following, the individual effects introduced by ρ_{sc} and r_a are discussed. As inferred from the data, it is expected that a surface coverage ρ_{sc} of ~0.10 is favourable to reduce sputter yields. In principle, this regime promotes a significant number of impinging ions to hit the sidewalls or the bottom surface next to the NCs, rather than the top region. If sputtered particles are emitted from these sites, they have a very high chance to get redeposited in the depths of the NCW structure. If the NC separation would be larger and thus ρ_{sc} smaller, the redeposition effect would decrease, as a larger solid angle towards vacuum becomes available for emission of sputtered particles, finally mimicking a flat surface. Vice versa, at larger ρ_{sc} the gaps between NCs become smaller. This trend leads to a higher chance that ion impacts are located closer to the NC top regions, which also reduces the redeposition capability of the NCW structure. In addition, when continuously reducing the separation distance, the NCs can start to overlap and therefore, a NCW structure would rather appear like a conventional rough surface, where rather the combination of redeposition and the variation of local ion incidence angles is influencing sputter yield[26,41]. A similar effect is responsible for the properties of those NCW surfaces which show a sputter yield enhancement under grazing ion incidence angle (θ = 80°, see Figure 3 (bottom)). Besides the projection towards the top regions, also the local surface inclination of NC tops shifts the local impact conditions towards lower θ, where sputter yields are higher (compare, e.g., the sputter yield tendency as a function of incidence angle for a flat W surface like in Figure 5(b)). Even though the sputter yield is actually increased for many NCW surfaces under grazing ion incidence, those configurations within the magenta-coloured ellipse still enabled a moderate reduction.

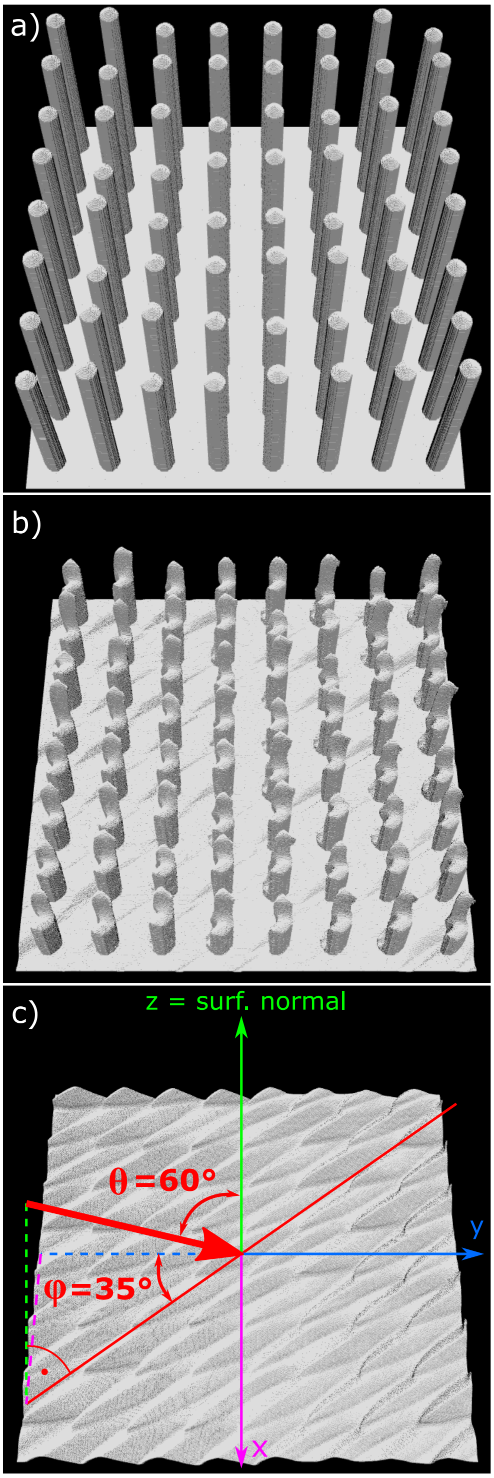

FIG. 6. Dynamic erosion of the optimised NCW surface under 2 keV Ar^+ bombardment with SDTrimSP-3D. a) initial NCW. b) NCW after 1.8×10^{21} $\mathrm{Ar/m^2}$. c) NCW after 4.0×10^{21} $\mathrm{Ar/m^2}$. In c), also the direction of ion irradiation is indicated ($\theta = 60°$ incidence angle with respect to the surface normal z, $\varphi = 35°$ azimuthal angle with respect to the y axis).

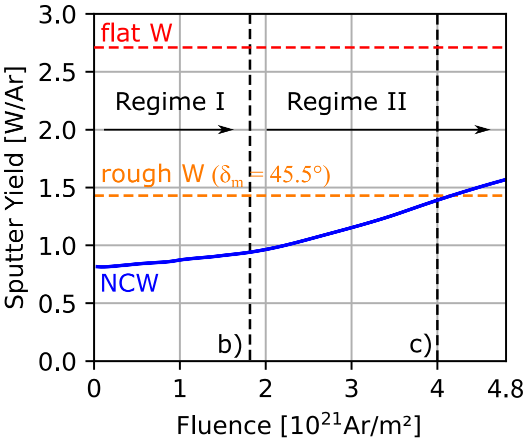

FIG. 7. Sputter yield evolution during dynamic erosion of the optimised NCW surface under 2 keV Ar^+ bombardment with incidence angle $\theta = 60°$, as simulated with SDTrimSP-3D. The slope of the data allows to separate the picture in two regimes (I and II). The dashed red line corresponds to the sputter yield of a flat W surface calculated by SDTrimSP-3D. Also a sputter yield for a conventionally rough W surface with a mean inclination angle δ_m=45.5° is included (predicted by the empirical fit formula in reference[26]). The vertical dashed black lines with labels b) and c) correspond to the fluence steps also displayed in Figures 6b) and c).

After discussing the effect of the surface coverage ρ_{sc}, more focus is put on the role of the aspect ratio r_a. Considering the trends for all investigated ion incidence cases, the lowest sputter yields were observed for $r_a \geq 10$, which indicates that the height of NCs has to be at least 10 times larger than their diameter to achieve the lowest possible sputter yield. For lower aspect ratios, the sputter yield reduction becomes gradually less efficient. If r_a is increased beyond 10, no significant additional advantage in sputter yield reduction is observed. Since creation of $r_a = 10$ was already achieved[18], we selected this value together with $\rho_{sc} = 0.10$ for further investigation, as these parameters show a good compromise between maintaining established technical aspects and optimal sputter yield reduction.

It has to be mentioned that the selection of ρ_{sc} and r_a is based solely on the empirical observations from our SPRAY simulations, which however include all geometric effects like variable local incidence conditions, redeposition, secondary sputtering (by projectiles that are first reflected and hit the NCW surface again) and shadowing. One option to further disentangle the individual contributions that led to the optimal geometric configuration would be to employ numerical tools that allow computation and visualisation of local particle fluxes on the topography. With such data at hand, it should be also possible to discuss the specific relation between the global incidence angle θ and ρ_{sc} in more detail. As another future step, analytical modelling of the sputtering behaviour in analogy to the work by P.S. Szabo et al.[42] would be desired and could support the selection of geometrical parameters as determined in the present work.

B. Comparison of MD, SPRAY and SDTrimSP-3D

In section III B, a general comparison of absolute sputter yield values based on MD allowed to substantiate results from the previous optimisation study, as the same trends in respect to ρ_{sc} and r_a were observed (see Figure 4). Together with the comparison of selected sputter yield data from all codes (SPRAY, MD, SDTrimSP-3D) as shown in Figure 5, these results support the selection of $\rho_{sc} = 0.10$ and $r_a = 10$ for investigation. Even though the absolute sputter yield values differed slightly between the codes, the general trends could be well reproduced. Especially the MD based results, which were obtained using much smaller NCs, further support the assumption that geometric properties of the NCW surface are the dominant cause of the sputter yield reduction. This is in line with the expectation that no transmission effects are relevant for our selected case of ion/target combination, where a mean projectile range of only 2.3 nm is predicted from SDTrimSP[30]. While some deviations between the values from individual codes are present in the data, it has to be mentioned that even for perfectly flat W surfaces the absolute sputter yield values vary between the codes[18].

While all used codes therefore support the optimum geometrical configuration of NCW for the presented case regarding 2 keV Ar^+ irradiation, it should be mentioned that this optimum may vary for other kinetic energies and choices of projectile/target species. These parameters are known to have a strong effect on sputter yields, ion reflection coefficients and the angular distribution of sputtered or reflected particles[43]. In this context, however, a numerical study by Eksaeva et al. revealed that also for similar sinusoidal Mo surface configurations, strong reductions in the sputter yield were predicted by the ERO2.0 code for 250 eV D irradiation under surface normal incidence[44]. Therefore, it is expected that strong sputter yield reductions can be also expected for NCW irradiation with more fusion-relevant fuel ions like for instance D.

C. Dynamic erosion of NCW

The slowly rising trend of the sputter yield over increasing fluence as shown in Figure 7 (for a NCW surface with $\rho_{sc} = 0.10$ and $r_a = 10$) is in good agreement with the data in Figure 3 (centre), which indicate a rising sputter yield trend for lower aspect ratios. Since the continuous dynamic erosion predominantly affected the NC height, the aspect ratio also decreased over fluence. Nevertheless, the reduced sputter yield prevailed relatively long and changed only marginally under this specific ion incidence angle of $\theta = 60°$, even though the overall erosion was already severe after a fluence of $\sim 1.8\times10^{21}$ Ar/m^2. At this point, also the bottom surface became directly visible for incoming ions. This behaviour supports that redeposition effects are still dominant in this regime. However, it can be observed that the sputter yield increase over fluence (i.e., the slope in the trend) became significantly steeper after this fluence was applied in the simulation. The increase coincided with a reduction of the NC aspect ratio r_a from initially 10 down to 6.3, due to the continuously reduced NC height. This value can be therefore seen as a characteristic r_a threshold value where a different erosion regime is entered (from regime I to II). While initially a strong sputter yield increase was also expected once the NCs are fully eroded ($\geq 4.0\times10^{21}$ Ar/m^2), surprisingly, a rather continuous behaviour was observed in this fluence regime. This is probably connected to the smooth erosion of the small remaining NC structures, while the underlying rippled topography gradually became dominant (see GIF video in the supplementary material). It is important to indicate that the specific development of erosion can differ for another choice of the ion incidence angle. Only a single case could be numerically investigated and presented in this work, due to computational constraints. However, a very similar step-wise erosion was already observed in other studies focusing on nano-columnar structures of tantalum (Ta) under Ar^+ bombardment, also employing SDTrimSP-3D[45]. Here, comparable structures evolved during similar applied fluences in both experiments and simulations. In addition, these results were analogously achieved using the ERO2.0 code, which therefore indicates a good agreement for the predicted dynamic evolution[46]. In addition, a final "ripple-surface" evolution (e.g., after prolonged ion irradiation of complex W-fuzz structures) was also found in previous experimental studies, justifying the relevance of our dynamically simulated final surface appearance[47]. The finally rippled topography could be also extracted from SDTrimSP-3D, allowing to interpolate height values at surface points located on a uniform lateral grid. With this, it was possible to deduce the mean inclination angle δ_m of the final surface. This parameter was identified as a reliable surface roughness metric, enabling to predict sputter yields of (Gaussian) rough surfaces[26,42]. A value of $\delta_m = 45.5°$ was deduced, which allows to estimate a sputter yield of Y = 1.43 W/Ar for 2 keV Ar^+ bombardment of rough W under 60° ion incidence angle (using the empirical fit formula in[26]). This value, which was added as dotted orange line to Figure 7, is in relatively good agreement with the final sputter yield simulated by SDTrimSP-3D in this work (Y = 1.58 W/Ar). The agreement suggests that the remaining reduction of the sputter yield in comparison to a flat W surface is due to known effects of conventional surface roughness.

As previously mentioned for ITER, total ion fluences up to 10^{31} ions/m^2 are expected, which therefore indicates a potential challenge for applying NCW surfaces as a coating for plasma facing components[6]. It has to be mentioned that conditions in a real fusion device are different than in our test case, where the dominant ion species, e.g., in the divertor, will rather correspond to deuterium, tritium and helium. Moreover, it is expected that these light ion species will have kinetic energies below the tungsten sputtering threshold (less than ∼200 eV for hydrogen isotopes[48]). Thus, only small abundances of higher-Z elements like the seeding gas species Ar can contribute to sputtering. Compared to our test case at 2 keV energy, the W sputter yield by Ar ions already drops to ∼10 % at 200 eV when simulated by SDTrimSP. Both a lower abundance (assuming ∼1 at.% similar to a study in JT-60U[49]) and the lower kinetic energy extend the expected overall fluence for full erosion of NCW by orders of magnitude (from $\sim 10^{21}$ towards $\sim 10^{24}$ ions/m^2), but it will remain a challenge to meet the desired fluence stability up to 10^{31} ions/m^2. One option could be to further decrease the kinetic energy of seeding gas species, closer to their W sputtering threshold energy, by increasing the abundance of seeding gas in the divertor. Still, the performance in terms of plasma discharge properties needs to be considered as well, which implies finding a good working point which meets all requirements[48]. Furthermore, larger aspect ratios than 10 (corresponding to higher NCs) can be another way to prolong the stability of the sputter yield reduction towards higher fluences during dynamic erosion. However, NCs with a height of several µm could penetrate the plasma sheath, which can trigger arcing events and thereby increase dust creation, similarly as observed by Kajita et al. for W-fuzz[14]. Instead of focusing only on erosion of *a-priori* created NCW surfaces, also the aspect of surface modification due to preferential sputtering could be relevant for a fusion device. Experimental erosion studies with materials having a mixed elemental composition indicated that needle-like surfaces may form during plasma exposition, which could in turn lead to favourable overall sputter yield reduction once established[19]. Besides, sputtering is not the only effect causing dynamic surface changes, e.g., W fuzz growth can be a critical aspect as well[14]. In this context, Qin et al. observed that similar NCW surfaces can retard W fuzz growth. However, the fluence regime after which W fuzz growth could be generally identified was well beyond 10^{24} ions/m^2 (for pure He plasma exposure below the sputtering threshold energy)[16]. Thus, the fuzz growth retardation may become substantially less effective if small amounts of higher-Z species with kinetic energies beyond the W sputtering threshold are present in the plasma of a fusion device. Under these conditions, erosion of NCW structures can happen even before retardation of W-fuzz growth becomes effective.

V. SUMMARY AND CONCLUSION

In this numerical study, three different simulation codes (SPRAY, SDTrimSP-3D and PARCAS) were used to optimise the sputter yield reduction properties of NCW surfaces for the case of 2 keV Ar$^+$ irradiation. To this end, the NCW geometry was varied by tuning the surface coverage density ρ_{sc} and the aspect ratio r_a, both being scale-independent parameters, to achieve the best reduction of sputter yields for a wide range of ion incidence angles. As a general trend, the reduction effect was enhanced for lower surface coverage densities and higher aspect ratios, which was supported by data from all codes. A key result was the identification of a promising geometrical regime with $\rho_{sc} \sim 0.10$ and $r_a \geq 10$, where large reductions by 80 % in comparison to the sputter yield for a flat W surface were achieved. Such a configuration is therefore of high interest for future developments regarding NCW, since such a sputter yield reduction would be favourable for applications in nuclear fusion devices. The actual growth of real NCW structures with a specific ρ_{sc} of 0.10 was not yet demonstrated and we indicate that this is an important topic for a future experimental study. Since the numerically optimised NCW surface shows large reduction of the sputter yield, testing new experimental methods for establishing the desired NCW configurations appears relevant. To further estimate the potential of NCW surfaces, the dynamic evolution during prolonged ion irradiation was simulated with SDTrimSP-3D. Generally, we observed that the sputter yield, even though rising during continuous erosion, remained well below the sputter yield of a flat W surface. It was also observed that in a first fluence regime, the sputter yield only slowly increases with rising fluence, which is accompanied by a continuous degradation of the NCs. Especially when the bottom of the NCW structure became directly exposed to the incident ions, the rate of sputter yield increase became faster, which indicated a second fluence regime. After a fluence of 4.0×10^{21} Ar/m^2, all NCs vanished and an oriented "ripple" topography remained, which can be described (in a limited frame) like a conventionally rough surface. Summarising, NCW surfaces have very promising and tunable sputtering characteristics which could qualify them for application in nuclear fusion devices. Still, further studies including simulations and experiments, especially focusing on dynamic erosion during plasma exposition under fusion-relevant conditions, are highly desired to finally pinpoint their applicability.

ACKNOWLEDGEMENTS

This work has been carried out within the framework of the EUROfusion Consortium, funded by the European Union via the Euratom Research and Training Programme (Grant Agreement No 101052200—EUROfusion). Views and opinions expressed are however those of the author(s) only and do not necessarily reflect those of the European Union or the European Commission. Neither the European Union nor the European Commission can be held responsible for them. Financial support has also been provided by KKKÖ (commission for the coordination of fusion research in Austria at the Austrian Academy of Sciences - ÖAW). The authors acknowledge TU Wien Bibliothek for financial support through its Open Access Funding Programme. Computer time granted by the IT Center for Science—CSC—Finland and the Finnish Grid and Cloud Infrastructure (persistent identifier urn:nbn:fi:research-infras-2016072533) is gratefully acknowledged. The research leading to these results has partially received funding from the Spanish Ministry of Science and Innovation, through the project RADIAFUS V, Grant No. PID2019-105325RB-C32, the Comunidad de Madrid (CAM) trough the projects Techno-Fusion (No. S2018/EMT-4437), and Convenio Plurianual con la Universidad Politécnica de Madrid en la línea de actuación Programa de Excelencia para el Profesorado Universitario of the CAM.

---

[*] cupak@iap.tuwien.ac.at

[1] J. Knaster, A. Moeslang, and T. Muroga, "Materials research for fusion," Nat. Phys. **12**, 424–434 (2016).

[2] V.P. Budaev, "Results of high heat flux tests of tungsten divertor targets under plasma heat loads expected in ITER and tokamaks (review)," Phys. Atom. Nuclei **79**, 1137–1162 (2016).

[3] J. Alvarez, A. Rivera, R. Gonzalez-Arrabal, D. Garoz, E. del Rio, and J.M. Perlado, "Materials Research for HiPER Laser Fusion Facilities: Chamber Wall, Structural Material and Final Optics," Fusion Sci. Technol. **60**, 565–569 (2011).

[4] Richard A Pitts, S Carpentier, F Escourbiac, T Hirai, V Komarov, S Lisgo, AS Kukushkin, A Loarte, M Merola, A Sashala Naik, *et al.*, "A full tungsten divertor for ITER: Physics issues and design status," Journal of Nuclear Materials **438**, S48–S56 (2013).

[5] Marius Wirtz, J Linke, Th Loewenhoff, G Pintsuk, and I Uytdenhouwen, "Transient heat load challenges for plasma-facing materials during long-term operation," Nucl. Mater. Energy **12**, 148–155 (2017).

[6] R.A. Pitts, X. Bonnin, F. Escourbiac, H. Frerichs, J. P. Gunn, T. Hirai, A. S. Kukushkin, E. Kaveeva, M. A. Miller, D. Moulton, V. Rozhansky, I. Senichenkov, E. Sytova, O. Schmitz, P. C. Stangeby, G. De Temmerman, I. Veselova, and S. Wiesen, "Physics basis for the first ITER tungsten divertor," Nucl. Mater. Energy **20**, 100696 (2019).

[7] J. Linke, J. Du, Th. Loewenhoff, G. Pintsuk, B. Spilker, I. Steudel, and M. Wirtz, "Challenges for plasma-facing components in nuclear fusion," Matter Radiat. Extremes **4**, 056201 (2019).

[8] C. P. Dhard, S. Brezinsek, M. Mayer, D. Naujoks, S. Masuzaki, D. Zhao, R. Yi, J. Oelmann, K. Schmid, J. Romazanov, C. Pardanaud, M. Kandler, A. K. Kharwandikar, G. Schlisio, O. Volzke, H. Grote, Y. Gao, L. Rudischhauser, A. Goriaev, T. Wauters, A. Kirschner, S. Sereda, E. Wang, M. Rasinski, T. Dittmar, G. Motojima, D. Hwangbo, S. Kajita, M. Balden, V. V. Burwitz, R. Neu, Ch. Linsmeier, and the W7-X Team, "Plasma-wall interaction studies in W7-X: main results from the recent divertor operations," Phys. Scr. **96**, 124059 (2021).

[9] A. Lahtinen, A. Hakola, J. Likonen, M. Balden, K. Krieger, S. Gouasmia, I. Bogdanovic Radovic, G. Provatas, M. Kelemen, S. Markelj, M. Pedroni, A. Uccello, E. Vassallo, D. Dellasega, M. Passoni, the ASDEX Upgrade Team, and the EUROfusion MST1 Team, "Influence of surface morphology on erosion of plasma-facing components in H-mode plasmas of ASDEX Upgrade," Nucl. Mater. Energy **33**, 101266 (2022).

[10] S. Brezinsek, A. Kirschner, M. Mayer, A. Baron-Wiechec, I. Borodkina, D. Borodin, I. Coffey, J. Coenen, N. den Harder, A. Eksaeva, C. Guillemaut, K. Heinola, A. Huber, V. Huber, M. Imrisek, S. Jachmich, E. Pawelec, M. Rubel, S. Krat, G. Sergienko, G.F. Matthews, A.G. Meigs, S. Wiesen, A. Widdowson, and and JET contributors, "Erosion, screening, and migration of tungsten in the JET divertor," Nucl. Fusion **59**, 096035 (2019).

[11] R. Neu, V. Bobkov, R. Dux, J. C. Fuchs, O. Gruber, A. Herrmann, A. Kallenbach, H. Maier, M. Mayer, T. Pütterich, V. Rohde, A. C. C. Sips, J. Stober, K. Sugiyama, and and ASDEX Upgrade Team, "Ten years of W programme in ASDEX Upgrade - challenges and conclusions," Phys. Scr. **2009**, T138 (2009).

[12] R. Neu, G. Arnoux, M. Beurskens, V. Bobkov, S. Brezinsek, J. Bucalossi, G. Calabro, C. Challis, J. W. Coenen, E. de la Luna, P. C. de Vries, R. Dux, L. Frassinetti, C. Giroud, M. Groth, J. Hobirk, E. Joffrin, P. Lang, M. Lehnen, E. Lerche, T. Loarer, P. Lomas, G. Maddison, C. Maggi, G. Matthews, S. Marsen, M.-L. Mayoral, A. Meigs, Ph. Mertens, I. Nunes, V. Philipps, T. Pütterich, F. Rimini, M. Sertoli, B. Sieglin, A. C. C. Sips, D. van Eester, G. van Rooij, and and JET-EFDA Contributors, "First operation with the JET International Thermonuclear Experimental Reactor-like wall," Phys. Plasmas **20**, 056111 (2013).

[13] G.S. Xu, L. Wang, D. M. Yao, G.Z. Jia, C.F. Sang, X.J. Liu, Y.P. Chen, H. Si, Z.S. Yang, H.Y. Guo, H.L. Du, Z.P. Luo, H. Li, Z.B. Zhou, L. Cao, H.C. Xu, T.J. Xu, Z.L. Wang, P.F. Zi, L. Li, L. Han, J.C. Xu, J.B. Liu, K.D. Li, B. Cao, Y.W. Yu, F. Ding, R. Ding, N. Yan, L.Y. Meng, Y.Q. Tao, H.Q. Wang, Y. Zhang, L.M. Shao, X.D. Zhang, S.Z. Zhu, B.N. Wan, and the EAST Team, "Physics design of new lower tungsten divertor for long-pulse high-power operations in EAST," Nucl. Fusion **61**, 126070 (2021).

[14] S. Kajita, N. Yoshida, and N. Ohno, "Tungsten fuzz: Deposition effects and influence to fusion devices," Nucl. Mater. Energy **25**, 100828 (2020).

[15] A. Terra, G. Sergienko, M. Gago, A. Kreter, Y. Martynova, M. Rasiński, M. Wirtz, Th. Loewenhoff, Y. Mao, D. Schwalenberg, L. Raumann, J. W. Coenen, S. Moeller, Th. Koppitz, D. Dorow-Gerspach, S. Brezinsek, B. Unterberg, and Ch. Linsmeier, "Micro-structuring of tungsten for mitigation of ELM-like fatigue," Phys. Scr. **2020**,

014045 (2020).

[16] W. Qin, F. Ren, R.P. Doerner, G. Wei, Y. Lv, S. Chang, M. Tang, H. Deng, C. Jiang, and Y. Wang, "Nanochannel structures in W enhance radiation tolerance," Acta Mater. **153**, 147–155 (2018).

[17] JF Ziegler, Jerome J Cuomo, and J Roth, "Reduction of ion sputtering yield by special surface microtopography," Appl. Phys. Lett. **30**, 268–271 (1977).

[18] Alvaro Lopez-Cazalilla, Christian Cupak, Martina Fellinger, Fredric Granberg, Paul Stefan Szabo, Andreas Mutzke, Kai Nordlund, Friedrich Aumayr, and Raquel González-Arrabal, "Comparative study regarding the sputtering yield of nanocolumnar tungsten surfaces under Ar^{+} irradiation," Phys. Rev. Mater. **6**, 075402 (2022).

[19] M Rasinski, S Möller, J Steffens, B Unterberg, K Sugiyama, T Schwarz-Selinger, A Kreter, and Ch Linsmeier, "Morphology and composition of fe–w coatings after deuterium plasma exposure as a model system for rafm steels," Phys. Scr. **2016**, 014013 (2016).

[20] Bernhard M Berger, Reinhard Stadlmayr, Dominic Bloech, Elisabeth Gruber, Kazuyoshi Sugiyama, Thomas Schwarz-Selinger, and Friedrich Aumayr, "Erosion of fe-w model system under normal and oblige d ion irradiation," Nucl. Mater. Energy **12**, 468–471 (2017).

[21] Alvaro Lopez-Cazalilla, Joonas Jussila, Kai Nordlund, and Fredric Granberg, "Effect of surface morphology on tungsten sputtering yields," Comput. Mater. Sci. **216**, 111876 (2023).

[22] Angel Barranco, Ana Borras, Agustin R Gonzalez-Elipe, and Alberto Palmero, "Perspectives on oblique angle deposition of thin films: From fundamentals to devices," Prog. Mater. Sci. **76**, 59–153 (2016).

[23] Raya El Beainou, Aurelio Garcia-Valenzuela, Marina Raschetti, Jean-Marc Cote, Rafael Alvarez, Alberto Palmero, Valérie Potin, and Nicolas Martin, "A 4-view imaging to reveal microstructural differences in obliquely sputter-deposited tungsten films," Mater. Lett. **264**, 127381 (2020).

[24] Aurelio García-Valenzuela, Rafael Alvarez, Victor Rico, Juan P Espinos, Maria C López-Santos, Javier Solís, Jan Siegel, Adolfo del Campo, Alberto Palmero, and Agustín R González-Elipe, "2D compositional self-patterning in magnetron sputtered thin films," Appl. Surf. Sci. **480**, 115–121 (2019).

[25] D Jonker, Z Jafari, JP Winczewski, C Eyovge, JW Berenschot, NR Tas, JGE Gardeniers, I De Leon, and A Susarrey-Arce, "A wafer-scale fabrication method for three-dimensional plasmonic hollow nanopillars," Nanoscale Advances **3**, 4926–4939 (2021).

[26] C. Cupak, Paul Stefan Szabo, H. Biber, R. Stadlmayr, C. Grave, M. Fellinger, J. Brötzner, Richard Arthur Wilhelm, W. Möller, A. Mutzke, M.V. Moro, and F. Aumayr, "Sputter yields of rough surfaces: Importance of the mean surface inclination angle from nano- to microscopic rough regimes," Appl. Surf. Sci. **570**, 151204 (2021).

[27] U. van Toussaint, A. Mutzke, A. Manhard, "Sputtering of rough surfaces: a 3D simulation study," Phys. Scr. **2017**, 014056 (2017).

[28] Kai Nordlund, N Runeberg, and D Sundholm, "Repulsive interatomic potentials calculated using hartree-fock and density-functional theory methods," Nucl. Instrum. Methods Phys. Res. B **132**, 45–54 (1997).

[29] G., de Temmerman and T., Hirai and R. A., Pitts, "The influence of plasma-surface interaction on the performance of tungsten at the ITER divertor vertical targets," Plasma Phys. Control. Fusion **60**, 45–54 (1997).

[30] A. Mutzke, R. Schneider, W. Eckstein, R. Dohmen, K. Schmid, U. von Toussaint, and G. Badelow, "SDTrimSP Version 6.00," IPP-Report Max-Planck-Institut für Plasmaphysik (2019).

[31] PS Szabo, D Weichselbaum, H Biber, C Cupak, A Mutzke, RA Wilhelm, and F Aumayr, "Graphical user interface for sdtrimsp to simulate sputtering, ion implantation and the dynamic effects of ion irradiation," Nucl. Instrum. Methods Phys. Res. B **522**, 47–53 (2022).

[32] Autodesk Inc., "Meshmixer, Website accessed on 2023-03-28, https://meshmixer.com/,".

[33] WD Wilson, LG Haggmark, and JP Biersack, "Calculations of nuclear stopping, ranges, and straggling in the low-energy region," Phys. Rev. B **15**, 2458 (1977).

[34] J Lindhard and M Scharff, "Energy dissipation by ions in the keV region," Phys. Rev. **124**, 128 (1961).

[35] Ordean S Oen and Mark T Robinson, "Computer studies of the reflection of light ions from solids," Nucl. Instrum. Methods **132**, 647–653 (1976).

[36] Mihai-Cosmin Marinica, Lisa Ventelon, MR Gilbert, L Proville, SL Dudarev, J Marian, G Bencteux, and F Willaime, "Interatomic potentials for modelling radiation defects and dislocations in tungsten," J. Phys. Condens. Matter **25**, 395502 (2013).

[37] H. J. C. Berendsen, J. P. M. Postma, W. F. van Gunsteren, A. DiNola, and J. R. Haak, "Molecular dynamics with coupling to an external bath," J. Chem. Phys. **81**, 3684–3690 (1984).

[38] A. Lopez-Cazalilla, A. Ilinov, F. Djurabekova, and K. Nordlund, "Modeling of high-fluence irradiation of amorphous Si and crystalline Al by linearly focused Ar ions," J. Phys. Condens. Matter **31**, 075302 (2018).

[39] A. Lopez-Cazalilla, F. Djurabekova, A. Ilinov, C. Fridlund, and K. Nordlund, "Direct observation of ion-induced self-organization and ripple propagation processes in atomistic simulations," Mater. Res. Lett. **8**, 110–116 (2020).

[40] K Schlueter, K Nordlund, Gerhard Hobler, M Balden, Fredric Granberg, O Flinck, TF Da Silva, and Rudolf Neu, "Absence of a crystal direction regime in which sputtering corresponds to amorphous material," Phys. Rev. Lett. **125**, 225502.

[41] M Küstner, W Eckstein, V Dose, and J Roth, "The influence of surface roughness on the angular dependence of the sputter yield," Nucl. Instrum. Methods Phys. Res. B **145**, 320–331 (1998).

[42] Paul Stefan Szabo, C Cupak, H Biber, N Jäggi, André Galli, Peter Wurz, and F Aumayr, "Analytical model for the sputtering of rough surfaces," Surf. Interfaces **30**, 101924 (2022).

[43] JP Biersack and W Eckstein, "Sputtering studies with the Monte Carlo program TRIM.SP," Applied Physics A **34**, 73–94 (1984).

[44] A Eksaeva, D Borodin, J Romazanov, A Kirschner, A Kreter, M Eichler, M Rasinski, A Pospieszczyk, B Unterberg, S Brezinsek, *et al.*, "Surface roughness effect on Mo physical sputtering and re-deposition in the linear plasma device PSI-2 predicted by ERO2.0," Nucl. Mater. Energy **19**, 13–18 (2019).

[45] Rodrigo Arredondo, *SIESTA: A new ion source setup and its application to erosion studies on first-wall materials for fusion reactors*, Ph.D. thesis, Technische Universität München (2019).

[46] Alina Eksaeva, D Borodin, J Romazanov, A Kreter, A Pospieszczyk, S Dickheuer, S Möller, B Göths, M Rasinski, U Knoche, *et al.*, "ERO2.0 modelling of the effects of surface roughness on molybdenum erosion and redeposition in the PSI-2 linear plasma device," Physica Scripta **2020**, 014057 (2020).

[47] R Stadlmayr, Paul Stefan Szabo, D Mayer, C Cupak, T Dittmar, L Bischoff, S Möller, M Rasiński, Richard Arthur Wilhelm, W Möller, *et al.*, "Sputtering of nanostructured tungsten and comparison to modelling with TRI3DYN," J. Nucl. Mater. **532**, 152019 (2020).

[48] Sebastijan Brezinsek, Andreas Kirschner, Matej Mayer, A Baron-Wiechec, Irina Borodkina, Dmitriy Borodin, I Coffey, J Coenen, Niek den Harder, Alina Eksaeva, *et al.*, "Erosion, screening, and migration of tungsten in the JET divertor," Nucl. Fusion **59**, 096035 (2019).

[49] H Urano, M Nakata, N Aiba, H Kubo, M Honda, N Hayashi, M Yoshida, Y Kamada, *et al.*, "Roles of argon seeding in energy confinement and pedestal structure in JT-60U," Nucl. Fusion **55**, 033010 (2015).